



Myeloperoxidase controls bone turnover by suppressing osteoclast differentiation through modulating reactive oxygen species level

Xiaoli Zhao¹, Shuai Lin¹, Huiying Li¹, Shuyi Si^{1*}, Zhen Wang^{1*}

¹Institute of Medicinal Biotechnology, Chinese Academy of Medical Sciences and Peking Union Medical College, Beijing 100050, China

*Corresponding author: Dr. Zhen Wang, Department of Biochemistry, Institute of Medicinal Biotechnology, Chinese Academy of Medical Sciences and Peking Union Medical College, Beijing 100050, China. Tel: 86-10-63165289. Email: wangzhen@imb.pumc.edu.cn; Dr. Shuyi Si, NHC Key Laboratory of Biotechnology of Antibiotics, Institute of Medicinal Biotechnology, Chinese Academy of Medical Sciences and Peking Union Medical College, Beijing 100050, China. Email: sisymb@hotmail.com;

Running title: Myeloperoxidase suppresses osteoclast differentiation

This article has been accepted for publication and undergone full peer review but has not been through the copyediting, typesetting, pagination and proofreading process which may lead to differences between this version and the Version of Record. Please cite this article as doi: 10.1002/jbmr.4215

Abstract

Myeloperoxidase (MPO) is a heme peroxidase that plays an important role in innate immunity for host defense against invading microorganisms by catalyzing hydrogen peroxide (H₂O₂)-mediated reactions. Although many reports indicate MPO exerts beneficial or detrimental effects on a variety of inflammatory diseases, little is known with regard to its functional role in bone homeostasis in vivo. Here, our work demonstrates that MPO was transcriptionally down-regulated in response to osteoclastogenic stimuli, and that exogenous alteration of MPO expression negatively regulated osteoclast (OC) differentiation in vitro. Genetic ablation of *Mpo* resulted in osteoporotic phenotypes and potentiated bone resorptive capacity in mice. Mechanistically, accumulation of intracellular H₂O₂ and reactive oxygen species (ROS) were observed in MPO deficiency, and MPO overexpression suppressed ROS production in mouse OC precursors. Moreover, a ROS scavenger Tempol inhibited the effect of MPO deficiency on OC formation and function as well as on receptor activator of nuclear factor- κ B ligand (RANKL)-initiated transduction signals activation including NF- κ B, mitogen-activated protein kinases (MAPKs) and Akt, indicating the increased ROS caused by MPO deficiency contributes to osteoclastogenesis. Taken together, our data demonstrate that MPO has a protective role in bone turnover by limiting osteoclastogenesis and bone resorption physiologically through modulating intracellular H₂O₂ level.

Keywords

Myeloperoxidase; osteoclast; bone; H₂O₂; Reactive Oxygen Species;

Introduction

The maintenance of bone homeostasis relies on the fine-tuned balance between bone formation and bone resorption ^(1,2). Disruption of the balance leads to various bone diseases including osteoporosis and osteosclerosis. Osteoclasts (OCs) possess the unique capacity to degrade the bone matrix both physiologically and pathologically, highlighting the importance for understanding the molecular mechanisms regulating their differentiation and function ^(1,3). OCs are derived from monocyte/macrophage lineage precursor cells in the bone marrow and specifically secrete acid and lytic enzymes including tartrateresistant acid phosphatase (TRAP) and Cathepsin K (CTSK) that affect bone turnover ⁽³⁾. Receptor activator of nuclear factor- κ B ligand (RANKL), upon binding to its receptor cognate RANK, is an essential regulator to initiate OC differentiation as well as the activation of several downstream signaling cascades, which include NF- κ B, mitogen-activated protein kinases (MAPKs) and phosphatidylinositol-3-kinase (PI3K) pathways, resulting in the activation of transcription factors such as nuclear factor of activated T cells, cytoplasmic 1 (NFATc1) to ultimately stimulate the expression of specific gene targets ⁽³⁻⁵⁾. Meanwhile, macrophage colony-stimulating factor (M-CSF), as a hematopoietic growth factor, plays a pivotal role in supporting the survival of OC precursors and works in concert with RANKL to activate the essential downstream targets during OC differentiation ⁽⁶⁾.

Myeloperoxidase (MPO) is a member of the superfamily of heme peroxidases that is mainly expressed in neutrophils, monocytes and tissue macrophages ⁽⁷⁾. As a component of the intracellular microbicidal system of phagocytes, MPO plays an important role in innate immunity for host defense against invading microorganisms by catalyzing hydrogen peroxide (H₂O₂)-mediated reactions. In the presence of H₂O₂, MPO is able to oxidize a halide to produce hypohalous acids, with hypochlorous acid (HOCl) being the most abundant one, in physiological conditions ⁽⁸⁾. Despite the well-established canonical neutrophil MPO-related oxidant destruction system upon infection, MPO has been widely implicated in the pathogenesis of multiple human inflammatory diseases, including cardiovascular diseases, inflammatory bowel disease, kidney disease, neuronal disease, pulmonary inflammation and metabolic syndrome ⁽⁹⁻¹³⁾. So far, many evidences in MPO-deficient animal models have shown the causal role between MPO initiated oxidation and various inflammatory disease processes are complicated, given that MPO is found to exert either pro- or anti-inflammatory effect under certain situations, and that both up- and down-regulation of MPO has been linked to disease risk ⁽⁷⁾. Intriguingly, although very limited evidence suggests the possible role of MPO in OC formation in vitro ⁽¹⁴⁾, the physiological and pathophysiological role of MPO in bone homeostasis has not been reported in vivo.

As MPO is capable of catalyzing the reaction to produce HOCl from H₂O₂ and Cl⁻, alterations of MPO expression or activity are found to have relevance with intracellular levels of H₂O₂ ^(15,16). Combined with the evidences showing that reactive oxygen species (ROS) (including mainly H₂O₂) play a pivotal role in the regulation of OC formation and function as the second messenger in receptor-mediated signaling transmission pathway ^(17,18), and that MPO gene expression occurs during the promyelocyte myeloid maturation stage in the bone marrow while decreased in fully differentiated myeloid cells ^(19,20), we speculate that endogenous MPO may be actively involved in regulation of OC differentiation as well as bone homeostasis.

In this study, we provide evidences for the first time that MPO deficiency promotes OC formation and decreases bone mass in vivo. Mechanistically, MPO regulated OC differentiation is mediated by the alterations of intracellular H₂O₂ levels that affect RANKL-initiated downstream signaling pathways in bone marrow macrophages (BMMs), the OC precursor cells. Together, our data demonstrate a novel protective role for MPO in bone homeostasis apart from its reported functions in inflammatory diseases.

Materials and Methods

Reagents and cell lines. Recombinant mouse soluble M-CSF and RANKL were purchased from PeproTech (Rocky Hill, NJ). Lipofectamine 2000 reagent and TRIZOL reagent were from Life Technologies (Carlsbad, CA). The PrimeScript RT reagent Kit was obtained from Takara Biotechnology (Shiga, Japan). Fast SYBR Green Master Mix and PowerUp™ SYBR Green Master Mix were from Thermo Fisher (Waltham, MA). DCFH-DA (2',7'-Dichlorofluorescein diacetate) powder was from Sigma-Aldrich and Tempol (4-Hydroxy-2,2,6,6-tetramethylpiperidinyloxy) was purchased from Selleckchem (Houston, TX). RAW264.7 macrophages were obtained from the Cell Center of Peking Union Medical College.

Animals. C57BL/6J mice (Wt) and MPO-deficient mice (*Mpo*^{tm1Lus}, Stock No: 004265) on C57BL/6J background were obtained from The Jackson Laboratory. All experimental animals were bred from *Mpo* heterozygote mothers, Wild-type mice, heterozygote KO mice, and homozygote knockout mice were genotyped by PCR, using two pairs of primers targeted at the knockout insertion sequence (F: 5'-AGG TCT CTA ACG CCA TCG TG-3'; R: 5'-CAC GAG ACT AGT GAG ACG TG-3') and WT gene (F: 5'-AGG TCT CTA ACG CCA TCG TG-3'; R: 5'-GTT GAG GCC AGT GAA GAA GG-3'). The mice were housed in a temperature- and humidity-controlled room and were allowed free access to standard chow diet and water before the experiments. The animal

study was approved by the Institutional Animal Care and Use Committee (IACUC) of Institute of Medicinal Biotechnology, Peking Union Medical College. We confirm that all the methods were performed in accordance with the relevant ethical guidelines and regulations.

Cell Culture. Bone marrow cells were obtained from the long bones of 18 week-old male mice which were sacrificed using ether anesthesia. The cells were centrifuged for 5 min. The precipitation was re-suspended with red blood cell lysis buffer and centrifuged again. Precipitated cells were suspended in α -MEM supplemented with 10% FBS and cultured for 24 h. Non-adherent cells were collected and cultured for 3 days in the presence of M-CSF (30 ng/mL). Floating cells were discarded and adherent cells were analyzed by flow cytometry using anti-CD11b antibody. Adherent cells were used as BMMs with the CD11b-positive proportion being more than 90%. BMMs were cultured in α -MEM supplemented with 10% FBS, 100 units/ml penicillin, 100 mg/l streptomycin, and 30 ng/ml M-CSF. RAW 264.7 cells were cultured in DMEM supplemented with 10% FBS, 100 units/ml penicillin and 100 mg/l streptomycin. For the induction of osteoclast differentiation, 50 ng/ml RANKL was used. In the cases of Tempol or NaNO₂ treatment, the compound was added simultaneously with RANKL.

Tartrate-resistant acid phosphatase (TRAP) and F-actin staining. RAW264.7 (3×10^3 cells/well) and BMMs (5×10^3 cells/well) were seeded in 96-well plates and stimulated with RANKL (50 ng/ml) for 5 days. Cells were subjected to TRAP staining as described⁽²¹⁾. TRAP-positive multinucleated cells (≥ 3 nuclei) were scored as osteoclasts. For F-actin staining, BMMs were seeded in 8-well chambered slides (Thermo Fisher Scientific) at the density of 10^4 cells per well and stimulated with RANKL for 5 days. BMMs were pre-cultured in α -MEM containing 30 ng ml M-CSF and 50 ng ml of RANKL for 3 days, the cells were regarded as mature OCs (mOCs). To determine F-actin rings formation of mOCs from Wt or *Mpo*^{-/-} BMMs, equal number of mOCs (10^4 cells/well) were further seeded in 8-well chambered slides and stimulated with RANKL

(50 ng/ml) for another 5 days. Cells were fixed and stained with TRITC-phalloidin working solution (red) (Yeasen, Shanghai, China) as described previously⁽²²⁾. Five random fields per sample were counted and averaged for each sample. Each experiment was performed in triplicates and repeated independently more than three times.

Bone matrix dissolution assay. BMMs (5×10^3 cells/well) were seeded in OsteoAssay Surface Plates (Corning Osteo-Assay Surface 96 wells) and then stimulated with RANKL (50 ng/ml) for 5 days. To determine bone resorption activity of mOCs from Wt or *Mpo*^{-/-} BMMs, equal number of mOCs (5×10^3 cells/well) were further seeded in osteoassay surface plates and stimulated with RANKL (50 ng/ml) for another 5 days. Then the cells were lysed with sodium hypochlorite for 5 min at room temperature, followed by washing twice with distilled water. Bone matrix dissolution were recorded using a microscope at 100x magnification. The images containing the dissolution area was analyzed by Image-Pro Plus 6.0 software (Media Cybernetics, Silver Spring, USA). Each experiment was performed in triplicates and repeated independently three times.

Microcomputed tomography (micro-CT) analysis. For micro-CT imaging, 18-week-old male mice (n = 5) were harvested and right femurs were collected for analysis. The micro-CT imaging was performed using Siemens Inveon CT/PET Multimodality system (Siemens Medical Solutions). The scanner was set at a voltage of 60 kV and a resolution of 10.32 μ m per pixel. Reconstructed images were analyzed on an Inveon Research Workplace (Siemens Medical Solutions) using manufacturer-supplied software. Trabecular bone area for the analysis was set from the closer margins at 0.5 mm to the further margins at 1.0 mm from the growth plate. The trabecular bone morphological parameters including bone volume fraction (BV/TV), trabecular number (Tb.N), trabecular thickness (Tb.Th), trabecular separation (Tb.Sp), specific bone surface (BS/BV) and trabecular bone pattern factor (Tb.Pf) were examined⁽²³⁾. Furthermore, we used TRAP staining to determine the OC surface/bone surface (OC.S/BS) by Image-Pro

Plus software. TRAP positive area was regarded as OC.S, and bone trabecular area was regarded as BS.

Enzyme-linked immunosorbent assay (ELISA). CTX-I and PINP level in the serum of the mice was measured using CTX-I ELISA kit (AC-06F1) and PINP ELISA kit (AC-33F1) from Immunodiagnostic Systems (Tyne and Wear, UK) according to the manufacturer's instructions.

Quantitative RT-PCR (qRT-PCR) analysis. Total RNA was extracted with TRIZOL reagent, and then reversely transcribed using PrimeScript RT Master Mix as described previously⁽²¹⁾. The PCR primers were listed as follows:

Mpo Primer F: 5'-TGACCAAGGACCAGGAGC-3';

Mpo Primer R: 5'-GCAGTTGAGGCCAGTGAAG-3';

Acp5 Primer F: 5'-AAATCACTCTTTAAGACCAG-3';

Acp5 Primer R: 5'-TTATTGAATAGCAGTGACAG-3'

Ctsk Primer F: 5'-CCTCTCTTGGTGTCCATAACA-3';

Ctsk Primer R: 5'-ATCTCTCTGTACCCTCTGCA-3';

Ocstamp Primer F: 5'-CTGTAACGAACTACTGACCCAGC-3';

Ocstamp Primer R: 5'-CCCAGGCTTAGGAAGACGAAG-3';

Nfatc1 Primer F: 5'-CCGTTGCTTCCAGAAAATAACA-3';

Nfatc1 Primer R: 5'-GTGGGATGTGAACTCGGAA-3';

Gapdh Primer F: 5'-CATGGCCTTCCGTGTTTCCTA-3';

Gapdh Primer R: 5'-CCTGCTTCACCACCTTCTTGAT-3'.

Immunoblotting (IB) analysis. IB analysis was performed as previously described⁽²¹⁾. The antibodies against MPO (ab208670) was purchased from Abcam (Abcam, Cambridge, UK). Antibodies against Phospho-P65 (#3033), P65 (#8242), Phospho-JNK (#4668), JNK (#9252), Phospho-ERK1/2 (#4370), ERK1/2 (#4695), Phospho-AKT

(#4060) and AKT(#4691) were obtained from cell signaling technology (CST, Danvers, USA). Antibodies against FLAG (F1804) and β -actin (A5441) were from Sigma-Aldrich (St. Louis, MO, USA). Horseradish peroxidase-linked secondary antibodies were purchased from Jackson ImmunoResearch (West Grove, PA, USA). Band densities of representative blots were determined with ImageJ software and normalized to the intensity of respective loading control β -actin in each lane.

Gene knockdown and overexpression. MPO-specific siRNA and negative control siRNA were generated by RIBOBio (Guangzhou, China). pCMV6-Mpo-FLAG and negative control cloning vector were purchased from OriGene (Rockville, MD, USA). RAW264.7 cells and BMMs were seeded into 96-well plates with 3000 cells/well or 5000 cells/well, and transfected into with 5 pmol siRNA or 100 or 200 ng pCMV6-Mpo using Lipofectamine 2000 according to the manufacturer's instructions. The *Mpo* siRNA target sequences were listed as follows:

- 1#: CCTGAATCCTCGATGGAAT;
- 2#: CCAATGACCCTCGAATCAA;
- 3#: GCCAAGGCCTTTCAATGTT.

Cell proliferation and TUNEL assay. Cells were seeded into 96-well plates with 5000 cells/well for 72 hours, and cell proliferation was tested by the ATPlite 1step kit (PerkinElmer, Waltham, MA) according to the manufacturer's instruction. The TUNEL Apoptosis Assay Kit (Sangon Biotech, Shanghai, China) was used to measure cellular apoptosis following the manufacturer's instructions. Cells were observed using a BX61 fluorescent microscope (Olympus Corporation, Tokyo, Japan). The number of positive cells per field was counted and the percentage of positive cells was calculated.

MPO activity assay. MPO activity was determined using Mpo Detection Kit (Nanjing Jiancheng Bioengineering Institute, China) according to the manufacturer's

instruction, and expressed as units per gram of total protein (μg). Total protein levels in the samples were analyzed using a BCA assay kit.

Hydrogen peroxide assay. The level of intracellular H_2O_2 was analyzed with a hydrogen peroxide assay kit (Beyotime Institute of Biotechnology, Shanghai, China) according to the manufacturer's instruction. Basically, cells were lysed in lysis buffer supplied by the kit. The supernatants were gathered by centrifuging at 12,000 g for 15 min. The supernatant of each sample (50 μL) was added to reaction reagent (100 μL) for 30 min at room temperature and measured immediately with a microplate reader (Bio-Rad) at a wavelength of 570 nm. The concentration of H_2O_2 was calculated using a standard curve generated with standard solutions of H_2O_2 and normalized to total protein levels determined with BCA assay. The level of serum H_2O_2 was similarly measured with the kit.

ROS Measurement. The cells were fixed in 4% formaldehyde for 15 min and then washed with PBS buffer. DCFH-DA (10 μM) was added to wells and incubated for 30 min at 37°C. The fluorescent intensity of individual cells was measured by fluorescence microscopy to detect the intracellular ROS level. The mean density from three independent experiments was quantified using Image-Pro Plus software.

RNA-seq and Bioinformatics analysis. Total RNA was isolated using TRIZOL reagent in Wt and *Mpo*^{-/-} BMMs. Two biological replicates were made in the Wt BMMs (C1 and C2) and *Mpo*^{-/-} BMMs (M1 and M2). The RNA quality was examined with an Agilent 2100 Bioanalyzer (Agilent Technologies, Santa Clara, CA, USA). The construction of an RNA-seq library was performed using a KAPA Stranded mRNA-Seq Kit for Illumina (KAPA Biosystems, Inc., Woburn, MA, USA) following the manufacturer's instructions. RNA-seq libraries were sequenced using an Illumina Novaseq 6000 (Microread Genetics Co. Ltd Beijing, China). RNA-seq data have been deposited in at the NCBI Sequence Read Archive - SRA at

<https://www.ncbi.nlm.nih.gov/sra> with accession numbers: PRJNA609772. Raw data were processed and filtered reads were mapped to *Mus musculus* genome (ftp://ftp.ensembl.org/pub/release-96/gtf/mus_musculus/) and genome annotation (ftp://ftp.ensembl.org/pub/release-96/fasta/mus_musculus/dna/) by HISAT (2.0.5-beta). FeatureCounts (Version 1.5.0-p1) was used to calculate gene expression. A list of differentially-expressed genes (DEGs) was identified using the R package “EdgeR”, and a p-value of 0.05 and $|\log_2(\text{fold-change})| > 1$ were set as thresholds for significance. GO and KEGG enrichment analyses of DEGs were implemented with KOBAS3.0. The expression of *Mpo* and osteoclast reporter genes was analyzed in GSE57468, GSE37219, and GSE125320 by GEO2R analysis.

Statistical analysis. Statistical analysis was performed with SPSS 17.0 (SPSS, Inc., Chicago, IL, USA). Data are presented for each figure in boxplots (show all points). Student’s *t* test was used for the comparison between two groups, while one-way analysis of variance (ANOVA) was used for comparison of more than two groups where needed. The Levene test was used to determine the homogeneity of the variances. LSD test was used when homogeneity was found and Tamhane’s T2 multiple comparison test was used when homogeneity was not found. The p values are shown up to $p = 0.10$.

Results

MPO expression is negatively linked to OC differentiation. We first analyzed several reported datasets that have relevance with positive or negative regulation of OC differentiation under different conditions, to try to find out whether MPO gene expression may be linked to OC formation⁽²⁴⁻²⁶⁾. Analysis of the dataset of GSE57468 retrieved from a study demonstrating the role of *Dim1* in OC formation indicates *Mpo* mRNA level is gradually decreased in mice BMMs in a time-dependent manner, while the expressions of OC biomarkers *Acp5* and *Ctsk* are significantly up-regulated during the transition of BMMs into OCs upon M-CSF and RANKL treatment (Fig. 1A)⁽²⁴⁾. In the data of

GSE37219 retrieved from *Nfatc1* conditional knockout mice, an increased tendency of *Mpo* expression in BMMs is observed, while *Acp5* and *Ctsk* expression levels along with other OC differentiation markers are decreased upon NFATc1 deficiency relative to the wild type (Wt) group during OC formation (Fig. 1B)⁽²⁵⁾. We further analyzed the GSE125320 data retrieved from an anterior cruciate ligament transection (ACLT) induced OA mouse model with enhanced osteoclastogenesis⁽²⁶⁾ and found downregulated expression of *Mpo* in ACLT-induced osteoarthritis (Fig. 1C, $p < 0.001$). To confirm this, we checked the *Mpo* mRNA level in RAW264.7 cells and BMMs isolated and purified from mice (Supplemental Fig. 1A) upon RANKL induction, and the gene is greatly decreased during the OC differentiation reflected by tartrate-resistant acid phosphatase (TRAP) positive staining (Fig. 1D; Supplemental Fig. 1B). Collectively, the evidences indicate lowered MPO expression coincides with RANKL-induced osteoclastogenesis under both basic and pathologic conditions.

Exogenous alteration of MPO expression affects OC differentiation in vitro.

Because MPO expression is down-regulated by RANKL, we asked if overexpression of the gene could directly suppress OC differentiation in vitro. To this end, we transfected a FLAG-tagged MPO cDNA construct into RAW264.7 cells and BMMs⁽²⁷⁾, and found efficient MPO overexpression markedly inhibited OC differentiation in RAW264.7 cells and BMMs upon RANKL or RANKL and M-CSF co-stimulation for 5 days, respectively, as evidenced by the significant reduction of TRAP positive multinucleated cells (Fig. 2A and B; Supplemental Fig. 2A and B). Conversely, upon efficient down-regulation of MPO expression by two siRNAs (2# and 3#), TRAP positive staining was greatly potentiated in both cells upon RANKL induction as compared with scramble control (Fig. 2C and D; Supplemental Fig. 2C and D). Supportively, quantitative RT-PCR analysis proved that the transcription levels of OC differentiation markers *Acp5*, *Ocstamp* and *Nfatc1* were all significantly elevated by MPO knockdown after RANKL stimulation

in RAW 264.7 cells relative to the scramble control (Fig. 2E). Therefore, the evidences indicate MPO expression negatively regulates OC differentiation in vitro.

MPO deficiency in mice displays lower bone mass and higher bone resorptive capacity. We next sought to characterize the physiological role of MPO on bone phenotypes in vivo using *Mpo* knockout male mice aged 18 weeks (*Mpo*^{-/-} mice). Gene and protein expression in bone tissues and BMMs as well as genotyping confirmed the ablation of MPO expression (Fig. 3A and 6A; Supplemental Fig. 3A). No significant differences were found with regard to the body weight (Supplemental Fig. 3B) and physical appearance of the animals between two groups (data not shown). Representative images of trabecular bone in femur by micro-CT analysis were shown in Fig. 3B, and the bone mass was greatly reduced in *Mpo*^{-/-} mice relative to Wt controls. Quantitative analyses revealed that bone morphological parameters including the trabecular bone volume fraction (BV/TV), trabecular thickness (Tb.Th) and trabecular number (Tb.N) were reduced by 38.6% ($p < 0.05$), 32.4% ($p < 0.01$) and 9.4%, respectively, while the trabecular separation increased (Tb.Sp), trabecular bone pattern factor (Tb.Pf) and specific bone surface (BS/BV) were enhanced by 29.3%, 168.7% ($p < 0.05$) and 49.4% ($p < 0.01$), respectively, in *Mpo*^{-/-} mice as compared with Wt controls (Fig. 3C). Decreased tendency of average cortical thickness (Ct.Th) was observed in *Mpo*^{-/-} mice as well (Supplemental Fig. 3C). We also compared the trabecular bone morphological parameters between *Mpo*^{-/-} and Wt groups of 18-week-old female and 18-month-old male mice. Similar osteoporotic phenotypes were observed upon MPO deficiency (Supplemental Fig. 4). Supportively, histological analysis revealed MPO deficiency caused apparently altered and loosened structure in the trabecular tissue (Fig. 3D). These data confirm MPO deficiency mimics significant osteoporotic phenotypes in vivo.

We further asked if the lowered bone mass in MPO deficient mice was due to the potentiation of bone resorptive capacity. Indeed, MPO deficient mice displayed

increased TRAP-positive surface in the histological sections of the femur relative to Wt groups (Fig. 3E). The serum level of collagen degradation product I (CTX-I), a bone resorption marker⁽²⁸⁾ was consistently found to be much higher in *Mpo*^{-/-} mice than that in the Wt counterparts (Fig. 3F). Meanwhile, little change of the serum level of propeptide of type I procollagen (PINP), a bone formation biomarker⁽²⁸⁾, was observed in *Mpo*^{-/-} mice (Fig. 3F).

Moreover, we extracted BMMs from both groups and compared their OC formation capacities. *Mpo*^{-/-} BMMs possess a higher capacity of OC differentiation and resorptive function than that from Wt group, as demonstrated by the increased TRAP staining and by analysis of F-actin belts as well as bone matrix dissolution upon M-CSF and RANKL co-treatment (Fig. 4A, left panel). Function of mature OCs (mOCs) were further compared and similar tendency was found (Fig. 4A, right panel). MPO over-expression in BMMs and mOCs from *Mpo*^{-/-} mice dramatically suppressed the up-regulated OC formation and function (Fig. 4B and C; Supplemental Fig. 5A). BMMs cellular proliferation and apoptosis was also analyzed with ATPlite assay and TUNEL staining, respectively. The growth rate was comparable between Wt and *Mpo*^{-/-} BMMs in response to M-CSF (Supplemental Fig. 5B). Moreover, little change was observed in apoptosis during OC differentiation from both groups (Supplemental Fig. 5C). This indicates the enhanced OC resorption capacity upon MPO deficiency is not due to altered progenitor numbers or viability. Collectively, the findings indicate that MPO has a protective role in bone metabolism by limiting osteoclastogenesis and bone resorption in vivo.

Accumulation of intracellular H₂O₂ and ROS upon MPO deficiency contributes to OC formation. We next investigated the potential mechanisms to address the regulatory role of MPO in OC differentiation. Since exon 7 containing the sequence encoding the heme binding capacity of MPO, which is responsible for its enzymatic activity as a peroxidase, was disrupted in *Mpo*^{-/-} mice⁽²⁹⁾, it was straightforward to test if MPO activity was changed in the *Mpo*-deficient BMMs. Indeed, the MPO activity was

greatly inhibited upon MPO deficiency (Fig. 5A). Ablation of MPO activity may result in the intracellular accumulation of H₂O₂, provided that the enzyme functions by catalyzing the reaction to produce HOCl by utilizing H₂O₂ and Cl⁻ (15,16). We consistently found much higher intracellular H₂O₂ level in *Mpo*^{-/-} BMMs than Wt controls upon M-CSF stimulation (Fig. 5B), while the total H₂O₂ in serum were comparable between the two groups (Supplemental Fig. 5D). Accordingly, increasing concentrations of H₂O₂ stimulated OC formation in BMMs (Fig. 5C). A MPO activity inhibitor NaNO₂, which is known to increase H₂O₂ (16), similarly potentiated OC formation in BMMs (Fig. 5D, Supplemental Fig. 6A) and RAW264.7 cells (Supplemental Fig. 6B). NaNO₂ had little effect on ALPL activity in osteoblastic cell line MC3T3-E1 cells upon induction (Supplemental Fig. 6C), indicating ablation of MPO activity has little effect on osteoblast differentiation.

Next, ROS generation was observed by DCFH-DA fluorescence staining during the OC differentiation in BMMs upon M-CSF and RANKL induction, which was further potentiated by MPO depletion (Fig. 5E). Moreover, MPO re-expression greatly abrogated the ROS generation in *Mpo*^{-/-} cells to a comparable level with that in the Wt group (Fig. 5E). To further validate the role of ROS in MPO-affected OC formation, we co-treated the *Mpo*-deficient BMMs with Tempol, a well-known ROS scavenger (30), and found Tempol indeed inhibited ROS, OC differentiation and function in *Mpo*^{-/-} group (Fig. 5F-H). Taken together, the findings indicate the production of intracellular H₂O₂ and ROS contributes to the OC formation and function by MPO deficiency.

ROS mediates MPO affected signals during OC differentiation. Intracellular signals essential for OC differentiation include RANKL-initiated activation of NF-κB, Akt, and MAPKs upon its binding to RANK (3). We tested if these signals might be regulated by MPO. In Fig. 6A, activating phosphorylation of NF-κB subunit p65, JNK, ERK1/2 and Akt signals were quickly observed upon RANKL stimulation in Wt BMMs, and the activated signals were all potentiated in the *Mpo*^{-/-} counterparts. Meanwhile, co-

treatment with Tempol showed an inhibitory tendency on the RANKL-initiated transduction signals activation in *Mpo*^{-/-} BMMs (Fig. 6B). Analysis of *Nfatc1* gene expression, a key transcription factor that functions downstream of NF-κB activation to regulate osteoclastogenesis⁽³⁾, demonstrated that MPO deficiency stimulated more *Nfatc1* expression than Wt control by RANKL induction, and either co-treatment with Tempol or overexpressing MPO greatly inhibited the stimulated *Nfatc1* mRNA level in *Mpo*^{-/-} group (Fig. 6C).

To further characterize gene expression patterns possibly affected by MPO, we performed genome-wide RNA sequencing analysis between Wt and *Mpo*^{-/-} BMMs. A total of 626 genes were found to be significantly up-regulated and 72 genes down-regulated in *Mpo*^{-/-} BMMs relative to Wt controls (Supplemental Table 1). The up-regulated gene sets were mainly enriched in those involved in immune response-related functions by Gene Ontology Biological Process (GO-BP) analysis (Fig. 6D; Supplemental Table 2), confirming the canonical role of MPO in innate immunity⁽⁷⁾. Interestingly, signaling pathway analysis by KEGG revealed that a panel of up-regulated genes by MPO deletion were enriched in the inflammatory signals such as NF-κB, MAPKs, and PI3K-Akt pathways (Fig. 6E; Supplemental Table 3), and the signal expressions were shown in Supplemental Fig. 7. The analysis confirms that MPO actively regulates host defense and inflammatory diseases by affecting relevant signaling pathways. Collectively, these data indicate MPO suppresses OC differentiation by inhibiting RANKL-initiated downstream signals, and H₂O₂ mediates the MPO-regulated OC signals after RANKL induction.

Discussion

Apart from the canonical function in host defense, MPO exerts complicated effects on a variety of inflammatory disease processes^(7,11,12), while little is known regarding its regulatory role in bone homeostasis. A recent work suggests that treatment with external

MPO inhibits the OC differentiation in human peripheral blood mononuclear cells and RAW264.7 cells in vitro ⁽¹⁴⁾. However, the work is rather descriptive and the physiological relevance of MPO in vivo and underlying mechanisms have not been clarified. Here, we demonstrate that MPO plays a pivotal protective role in bone remodeling by suppressing osteoclastogenesis in vivo and in vitro, and that MPO genetic ablation results in osteoporosis in mice. Molecular profiling of OC precursors reveals H₂O₂ accumulation by MPO deficiency contributes to the potentiated OC differentiation and transduction signals.

OC differentiation is regulated by external cytokines including M-CSF and RANKL, which bind to their respective receptors and initiate multiple signal transduction pathways to activate several transcriptional factors such as NF- κ B and NFATc1 in myeloid progenitors ⁽³⁻⁵⁾, resulting in expression of OC differentiation markers such as *Acp5*, *Ocstamp* and *Ctsk*. Several datasets analyzes reveal MPO expression is negatively linked to OC differentiation under both basic and pathological conditions (Fig. 1). We also observed that *Mpo* is transcriptionally down-regulated during OC differentiation in vitro (Fig. 1D). The finding is consistent with the notion that *Mpo* gene expression normally occurs in myeloid precursors in bone marrow ⁽¹⁹⁾, but rapidly decreases upon cellular differentiation and becomes undetectable in mature phagocytes in circulation or tissue ⁽²⁰⁾. As OCs are unlikely to contain MPO at the mature and bone resorbing stage, we speculate that the checkpoint function of MPO occurs at the differentiation level in the OC precursors.

Our findings indicate that MPO has a protective role in bone turnover by limiting osteoclastogenesis and bone resorption, as evidenced by (a) down- and up-regulation of MPO expression potentiates and suppresses OC differentiation in vitro, respectively (Fig. 2 and 4; Supplemental Fig. 2); (b) MPO deficiency in mice displays reduced bone mass and higher bone resorptive capacity (Fig. 3); and (c) MPO deficiency potentiates the RANKL-initiated transduction signals activation including NF- κ B, MAPKs and Akt (Fig.

6A and B). Moreover, we found MPO exerts little effect on osteoblast formation, and the observation is consistent with a previous study, which checked the osteogenic role of a panel of peroxidase enzymes in vitro ⁽³¹⁾. This suggests MPO might mainly function to control the resorptive process during bone homeostasis.

Many reports suggest a functional MPO promoter polymorphism, -463GA, in the Alu receptor response element (AluRRE) has been associated with the regulation of its myeloid-specific expression level in many diseases ^(10,11). Moreover, peroxisome proliferator-activated receptor γ (PPAR γ) and estrogen receptor also mediate the up- and down-regulation of *MPO* gene expression through the AluRRE upon different stimuli in human myeloid cells ⁽³²⁾. However, due to the lack of AluRRE sequence in murine *Mpo* gene ⁽³²⁾, further studies are needed to elucidate the molecular basis to address the observed transcriptional repression of MPO in OC progenitors during differentiation process.

The physiological and pathological functions of MPO are usually accompanied by oxidant stresses ⁽¹¹⁾. As MPO functions by reacting with chloride and H₂O₂ to produce a powerful oxidant HOCl, blocking its activity usually results in the accumulation of intracellular H₂O₂ ^(15,16). Indeed, our work confirms much lower enzymatic activity and higher intracellular H₂O₂ as well as ROS production in MPO-deficient BMMs relative to Wt control, while MPO re-expression suppresses the ROS generation in the OC precursors (Fig. 5). H₂O₂, as a primary ROS type, plays an important role in regulating OC formation, function and RANKL-initiated downstream signaling events including NF- κ B, MAPKs and PI3K ^(17,18,33). Our analysis proves the increased ROS generation by MPO deficiency contributes to osteoclastogenesis based on observations that (a) treatment with H₂O₂ mimics the effect of MPO depletion on OC formation; (b) MPO inhibitor NaNO₂ known to increase H₂O₂ enhances OC formation; (c) scavenger of ROS by Tempol or MPO re-expression fully abrogates the effect of MPO deficiency on OC formation, function and RANKL-initiated transduction signals (Fig. 4-6). Interestingly, as

HOCl is reported to be a potential inhibitor of NF- κ B⁽³⁴⁾, the possible effect of decreased HOCl level upon MPO deficiency on the inflammatory signals during OC formation might not be excluded.

Finely-tuned ROS generation is a necessary step to maintain normal osteoclast differentiation^(17,18). The NADPH oxidases (NOXs) family are known to be major ROS enzymatic sources and RANKL initiated RANK-TRAF6-Rac1-NOXs signaling cascade, along with mitochondria, is suggested to contribute to the ROS production during OC differentiation^(17,18). Our study indicates that MPO, possibly with other heme peroxidases, constitutes an important enzyme that physiologically and delicately helps regulate ROS dynamic balance during bone homeostasis without causing a significant effect on cell death of OCs.

MPO knockout mice, although vital, exhibit increased susceptibility to certain types of infection as well as detrimental or beneficial phenotypes in different tissues or organs under a host of pathological stresses, therefore reflecting the complicity of its physiological and pathophysiological functions. Our findings in this work demonstrate that MPO functions as an important checkpoint protein that controls skeletal turnover by restraining osteoclastogenesis and bone resorption. The study reveals a beneficial role of MPO in bone homeostasis and expands our understanding of its biological importance beyond the well-established functions.

Disclosure

All the authors declare no conflicts of interest.

Acknowledgments

This work is supported by grants from the Drug Innovation Major Project from Ministry of Science and Technology of China (No. 2018ZX09711001-003-006 to ZW),

CAMS Innovation Fund for Medical Sciences (No. 2016-I2M-2-002 to ZW) and Fundamental Research Funds for the Central Universities (No. 3332019081 to XLZ).

Authors' roles: X. Z. and Z. W. designed the study; X. Z., S. L. and H. L. performed the work; X. Z., S. L., H. L., S. S. and Z. W. analyzed and interpreted the data; and X. Z., S. S. and Z. W. wrote and revised the paper. All authors reviewed and approved the manuscript.

References

1. Lorenzo J. The many ways of osteoclast activation. *The Journal of clinical investigation*. 2017;**127**(7):2530-2.
2. Segovia-Silvestre T, Neutzsky-Wulff AV, Sorensen MG, Christiansen C, Bollerslev J, Karsdal MA, et al. Advances in osteoclast biology resulting from the study of osteopetrotic mutations. *Human genetics*. 2009;**124**(6):561-77.
3. Boyle WJ, Simonet WS, Lacey DL. Osteoclast differentiation and activation. *Nature*. 2003;**423**(6937):337-42.
4. Takayanagi H. Osteoimmunology: shared mechanisms and crosstalk between the immune and bone systems. *Nat Rev Immunol*. 2007;**7**(4):292-304.
5. Yang M, Birnbaum MJ, MacKay CA, Mason-Savas A, Thompson B, Odgren PR. Osteoclast stimulatory transmembrane protein (OC-STAMP), a novel protein induced by RANKL that promotes osteoclast differentiation. *Journal of Cellular Physiology*. 2008;**215**(2):497-505.
6. Tanaka S, Nakamura K, Takahashi N, Suda T. Role of RANKL in physiological and pathological bone resorption and therapeutics targeting the RANKL-RANK signaling system. *Immunol Rev*. 2005;**208**:30-49.
7. Aratani Y. Myeloperoxidase: Its role for host defense, inflammation, and neutrophil function. *Archives of Biochemistry and Biophysics*. 2018;**640**:47-52.

8. Rayner BS, Love DT, Hawkins CL. Comparative reactivity of myeloperoxidase-derived oxidants with mammalian cells. *Free Radical Biology and Medicine*. 2014;**71**:240-55.
9. Vanhamme L, Zouaoui Boudjeltia K, Van Antwerpen P, Delporte C. The other myeloperoxidase: Emerging functions. *Archives of Biochemistry and Biophysics*. 2018;**649**:1-14.
10. Nauseef WM. Biosynthesis of human myeloperoxidase. *Archives of Biochemistry and Biophysics*. 2018;**642**:1-9.
11. Ndrepepa G. Myeloperoxidase – A bridge linking inflammation and oxidative stress with cardiovascular disease. *Clinica Chimica Acta*. 2019;**493**:36-51.
12. Chami B, Martin NJJ, Dennis JM, Witting PK. Myeloperoxidase in the inflamed colon: A novel target for treating inflammatory bowel disease. *Archives of Biochemistry and Biophysics*. 2018;**645**:61-71.
13. Pravalika K, Sarmah D, Kaur H, Wanve M, Saraf J, Kalia K, et al. Myeloperoxidase and Neurological Disorder: A Crosstalk. *ACS Chem Neurosci*. 2018;**9**(3):421-30.
14. Panagopoulos V, Liapis V, Zinonos I, Hay S, Leach DA, Ingman W, et al. Peroxidase enzymes inhibit osteoclast differentiation and bone resorption. *Molecular and Cellular Endocrinology*. 2017;**440**:8-15.
15. Winterbourn CC, Hampton MB, Livesey JH, Kettle AJ. Modeling the reactions of superoxide and myeloperoxidase in the neutrophil phagosome: implications for microbial killing. *The Journal of biological chemistry*. 2006;**281**(52):39860-9.
16. van Dalen CJ, Winterbourn CC, Senthilmohan R, Kettle AJ. Nitrite as a substrate and inhibitor of myeloperoxidase. Implications for nitration and hypochlorous acid production at sites of inflammation. *The Journal of biological chemistry*. 2000;**275**(16):11638-44.

17. Agidigbi TS, Kim C. Reactive Oxygen Species in Osteoclast Differentiation and Possible Pharmaceutical Targets of ROS-Mediated Osteoclast Diseases. *International Journal of Molecular Sciences*. 2019;**20**(14):3576.
18. Callaway DA, Jiang JX. Reactive oxygen species and oxidative stress in osteoclastogenesis, skeletal aging and bone diseases. *Journal of Bone and Mineral Metabolism*. 2015;**33**(4):359-70.
19. Lubbert M, Miller CW, Koeffler HP. Changes of DNA methylation and chromatin structure in the human myeloperoxidase gene during myeloid differentiation. *Blood*. 1991;**78**(2):345-56.
20. Lin KM, Austin GE. Functional activity of three distinct myeloperoxidase (MPO) promoters in human myeloid cells. *Leukemia*. 2002;**16**(6):1143-53.
21. Zhao XL, Chen JJ, Si SY, Chen LF, Wang Z. T63 inhibits osteoclast differentiation through regulating MAPKs and Akt signaling pathways. *European journal of pharmacology*. 2018;**834**:30-5.
22. Zhao XL, Chen LF, Wang Z. Aesculin modulates bone metabolism by suppressing receptor activator of NF-kappaB ligand (RANKL)-induced osteoclastogenesis and transduction signals. *Biochemical and biophysical research communications*. 2017;**488**(1):15-21.
23. Buxsein ML, Boyd SK, Christiansen BA, Guldberg RE, Jepsen KJ, Muller R. Guidelines for assessment of bone microstructure in rodents using micro-computed tomography. *Journal of bone and mineral research*. 2010;**25**(7):1468-86.
24. An D, Kim K, Lu W. Defective entry into mitosis 1 (Dim1) negatively regulates osteoclastogenesis by inhibiting the expression of nuclear factor of activated T-cells, cytoplasmic, calcineurin-dependent 1 (NFATc1). *The Journal of biological chemistry*. 2014;**289**(35):24366-73.

25. Aliprantis AO, Ueki Y, Sulyanto R, Park A, Sigrist KS, Sharma SM, et al. NFATc1 in mice represses osteoprotegerin during osteoclastogenesis and dissociates systemic osteopenia from inflammation in cherubism. *The Journal of clinical investigation*. 2008;**118**(11):3775-89.
26. Ren X, Hu B, Song M, Ding Z, Dang Y, Liu Z, et al. Maintenance of Nucleolar Homeostasis by CBX4 Alleviates Senescence and Osteoarthritis. *Cell reports*. 2019;**26**(13):3643-56 e7.
27. Weischenfeldt J, Porse B. Bone Marrow-Derived Macrophages (BMM): Isolation and Applications. *CSH protocols*. 2008;**2008**:pdb prot5080.
28. Szulc P, Naylor K, Hoyle NR, Eastell R, Leary ET, for the National Bone Health Alliance Bone Turnover Marker P. Use of CTX-I and PINP as bone turnover markers: National Bone Health Alliance recommendations to standardize sample handling and patient preparation to reduce pre-analytical variability. *Osteoporosis International*. 2017;**28**(9):2541-56.
29. Battistuzzi G, Bellei M, Bortolotti CA, Sola M. Redox properties of heme peroxidases. *Arch Biochem Biophys*. 2010;**500**(1):21-36.
30. Wilcox CS, Pearlman A. Chemistry and antihypertensive effects of tempol and other nitroxides. *Pharmacological reviews*. 2008;**60**(4):418-69.
31. DeNichilo MO, Shoubridge AJ, Panagopoulos V, Liapis V, Zysk A, Zinonos I, et al. Peroxidase Enzymes Regulate Collagen Biosynthesis and Matrix Mineralization by Cultured Human Osteoblasts. *Calcified tissue international*. 2016;**98**(3):294-305.
32. Kumar AP, Piedrafita FJ, Reynolds WF. Peroxisome proliferator-activated receptor gamma ligands regulate myeloperoxidase expression in macrophages by an estrogen-dependent mechanism involving the -463GA promoter polymorphism. *The Journal of biological chemistry*. 2004;**279**(9):8300-15.

33. Kim HS, Nam ST, Mun SH, Lee S-K, Kim HW, Park YH, et al. DJ-1 controls bone homeostasis through the regulation of osteoclast differentiation. *Nature Communications*. 2017;**8**(1):1519.
34. Gloire G, Legrand-Poels S, Piette J. NF- κ B activation by reactive oxygen species: Fifteen years later. *Biochemical Pharmacology*. 2006;**72**(11):1493-505.

Figure legends

Figure 1. MPO expression during OC differentiation. (A) Gene expression changes of *Mpo*, *Acp5* and *Ctsk* in mouse BMMs from dataset GSE57468, with RANKL and M-CSF co-stimulation at the indicated time (n = 2). The p values were determined using one way ANOVA with LSD comparison test. (B) Gene analysis of wild type (Wt) and NFATc1-deficient (*Nfatc1*^{-/-}) BMMs (GSE37219) during OC formation (n = 2). (C) Transcriptome analysis of knee joints tissues in ACLT-induced osteoarthritis mice model from dataset GSE125320 (n = 3). (D) RAW264.7 cells were induced with RANKL (50 ng/ml) for 4 days followed by TRAP staining (left panel) and qRT-PCR analysis (right panel) (n = 3 independent experiments). Scale bar = 50 μ m. The p values (B&D) were determined using Student's *t* test.

Figure 2. Effect of MPO expression on OC differentiation in RAW264.7 cells. (A) Cells were transfected with increasing amounts of pCMV6-Mpo-FLAG (0, 2.5 and 5.0 μ g) for 72 h followed by Immunoblotting (IB) analysis. Results were representative from three independent experiments. (B) Cells were transfected with the plasmid for 6 h before treatment with RANKL for 5 days, followed by TRAP staining (n = 5 independent experiments). The p values were determined using one way ANOVA with LSD comparison test. Scale bar = 50 μ m. (C) Cells were transfected with scrambled or *Mpo* siRNA for 72 h, followed by MPO protein and mRNA analysis (n = 3 independent experiments). (D) TRAP staining of the siRNA-transfected cells after RANKL induction.

The number of TRAP positive multinucleated cells was scored (n = 3 independent experiments). Scale bar = 50 μ m. (E) Expression of the osteoclastogenesis-related genes in the siRNA-transfected cells by qRT-PCR (n = 6 independent experiments). The p values in (C-E) were determined using Student's *t* test.

Figure 3. MPO regulates bone mass and bone resorptive capacity in mice. (A) Comparison of *Mpo* mRNA in the femur tissues of Wt and *Mpo*^{-/-} groups (n = 3 mice). (B) Representative micro-CT images of trabecular bone from 18-week-old Wt and *Mpo*^{-/-} male mice (n = 5). Scale bar = 0.5 mm. (C) Quantification of bone morphological parameters as indicated (n = 5 mice). (D) Representative images of H&E staining in femur tissues of the two groups (n = 5 mice). Scale bar = 250 μ m. (E) Representative images of TRAP staining in femur tissues. Arrows indicated TRAP-positive staining areas. Scale bar = 50 μ m. The osteoclast surface per bone surface (OC.S/BS) was shown (n = 5 mice). (F) Measurement of serum CTX-I and PINP level (n = 5 mice). The p values were determined using Student's *t* test.

Figure 4. Comparison of OC differentiation and function in Wt and MPO-deficient BMMs. (A) Representative images of TRAP staining, F-actin belts and bone matrix dissolution in BMMs and mOCs stimulated by M-CSF and RANKL from three independent experiments (upper panel). Respective quantification is shown in the lower panel). Scale bar = 50 μ m. (B) MPO expression by IB analysis and representative images of TRAP staining in Wt, *Mpo*^{-/-} and *Mpo*^{-/-} BMMs with MPO overexpression, upon M-CSF and RANKL induction (n = 3 independent experiments). *Mpo*^{-/-} BMMs were transfected with pCMV6-Mpo-FLAG for 6 h before treatment with M-CSF and RANKL for 5 days. Scale bar = 50 μ m. (C) MPO expression by IB analysis and representative images of bone resorption. Quantification from three independent experiments is shown in the right. Wt and *Mpo*^{-/-} BMMs were overexpressed with MPO as above. The p values were determined using Student's *t* test.

Figure 5. Accumulation of intracellular H₂O₂ and ROS by MPO deficiency contributes to OC differentiation and function. (A) MPO activity in BMMs from Wt and *Mpo*^{-/-} mice (n = 3 independent experiments). (B) Intracellular H₂O₂ levels in Wt and *Mpo*^{-/-} BMMs upon M-CSF induction (n = 4 independent experiments). (C) TRAP positive OCs in Wt BMMs after treatment with H₂O₂ in presence of M-CSF and RANKL for 5 days (n = 3 independent experiments). (D) Wt BMMs were treated with NaNO₂ in presence of M-CSF and RANKL for 5 days, followed by TRAP staining (n = 3 independent experiments). Scale bar = 50 μm. (E) Representative images and quantification for DCFH-DA fluorescence intensity in Wt and *Mpo*^{-/-} BMMs transfected with indicated vectors in the presence of M-CSF and RANKL from three independent experiments. Scale bar = 10 μm. (F-H) The *Mpo*^{-/-} BMMs or mOCs were treated with 30 μM Tempol in the presence of M-CSF and RANKL, followed by DCF staining, TRAP staining and bone matrix dissolution analysis (n = 3 independent experiments). The p values were determined using Student's *t* test (A, B, E-H) and one way ANOVA with LSD comparison test (C-D).

Figure 6. MPO regulates RANKL-initiated transduction signals in OC differentiation. (A) IB analysis of RANKL-stimulated OC signals in Wt or *Mpo*^{-/-} BMMs from three independent experiments. Wt and *Mpo*^{-/-} BMMs were treated with M-CSF and RANKL for the indicated time and subjected to IB analysis. (B) IB analysis of OC signals in Wt and *Mpo*^{-/-} BMMs after RANKL treatment for 30 min from three independent experiments. Tempol (30 μM) was added into *Mpo*^{-/-} BMMs along with RANKL induction for comparison. The band densities were quantified in the lower panel. (C) *Nfatc1* mRNA expression by qRT-PCR from three independent experiments. *Mpo*^{-/-} BMMs were treated with 30 μM Tempol or transfected with pCMV6-Mpo (2.5 μg) in the presence of M-CSF and RANKL (n = 3 independent experiments). The p values were determined using Student's *t* test. (D and E) Gene Ontology Biological Process and

KEGG pathways enrichment analysis of the upregulated genes in MPO-deficient BMMs compared to Wt BMMs from RNA sequencing data.

Figure 1

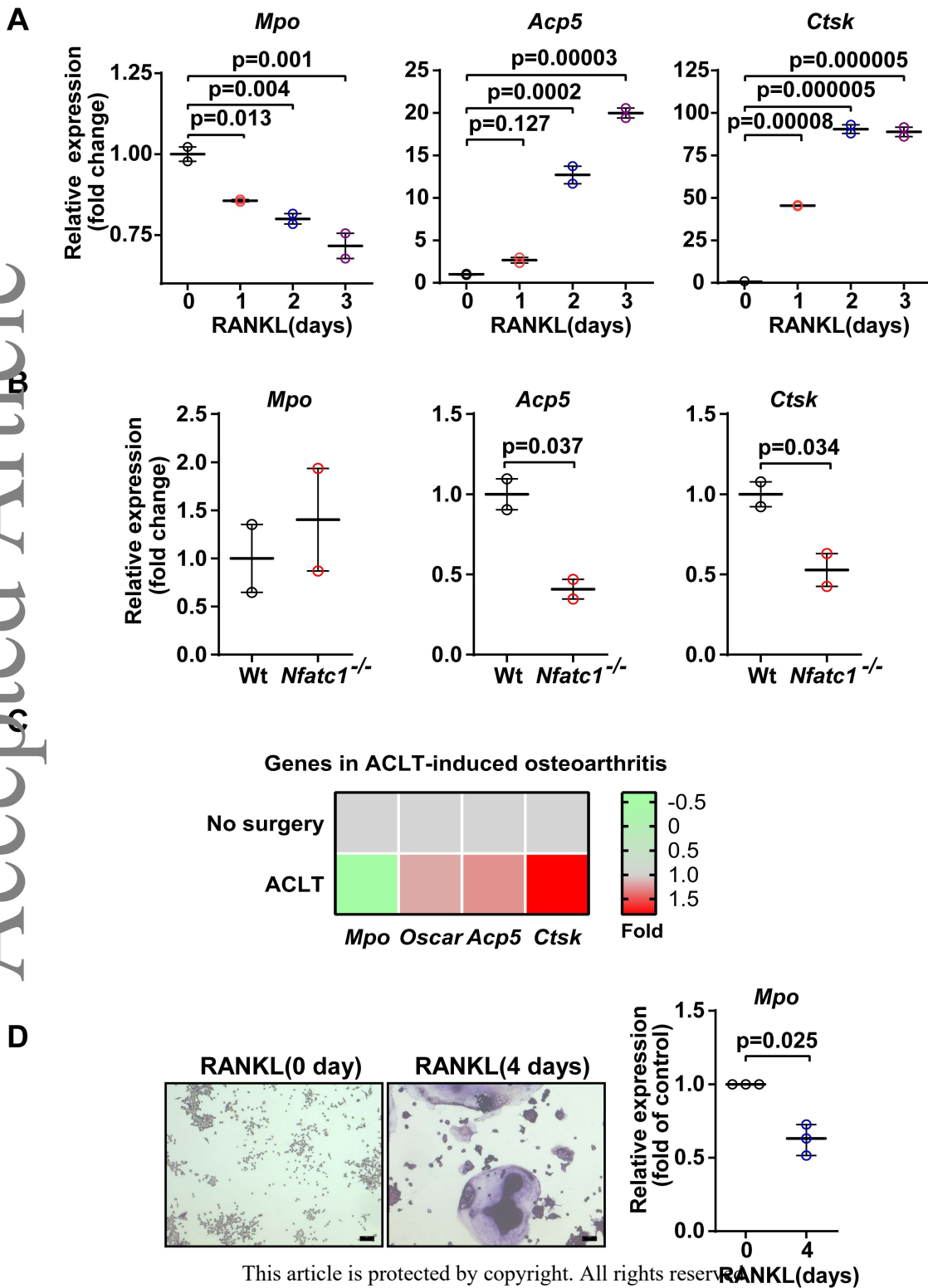
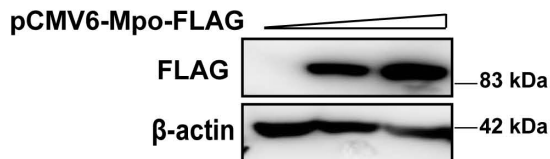


Figure 2

A



B

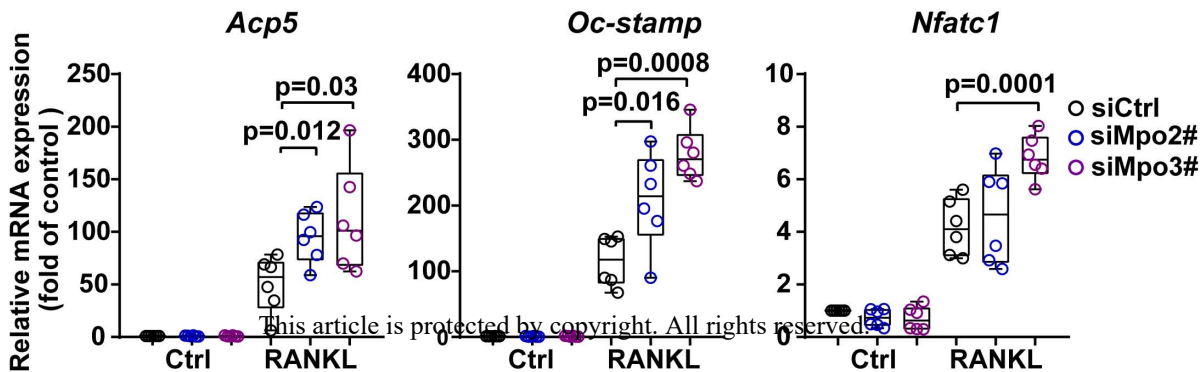
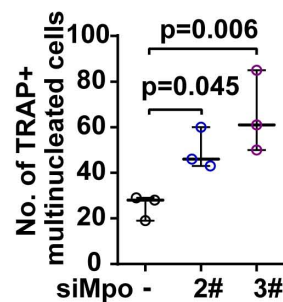
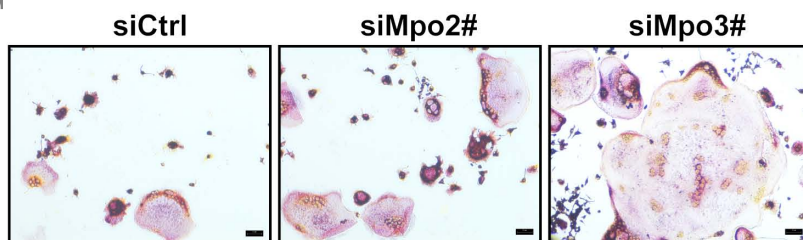
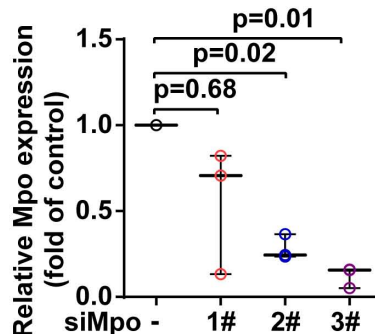
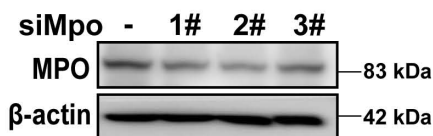
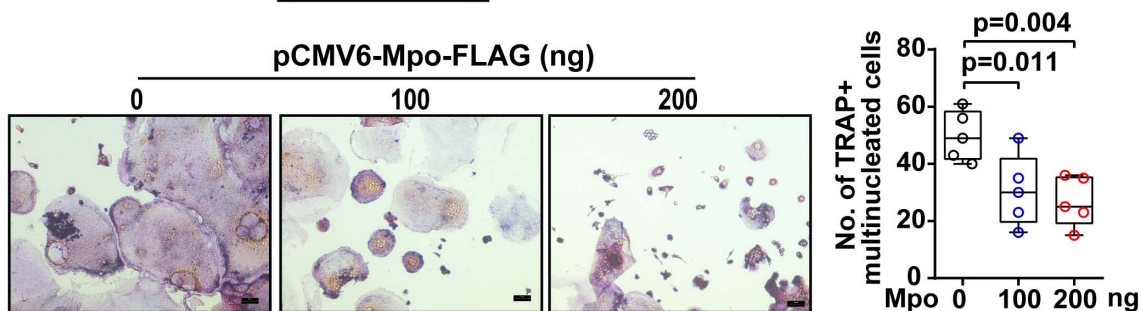
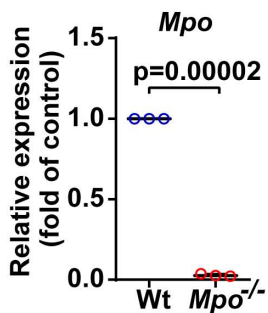
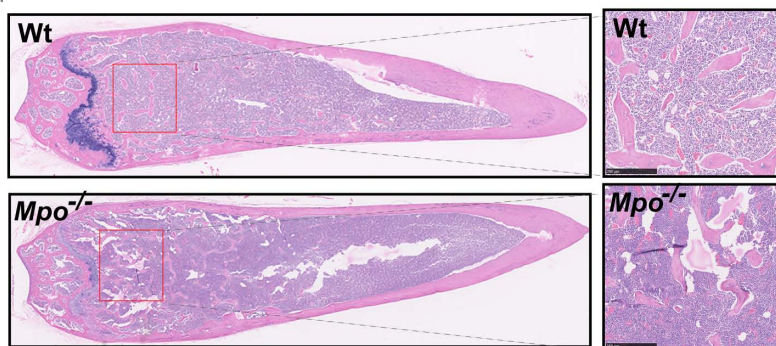
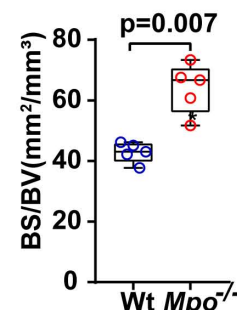
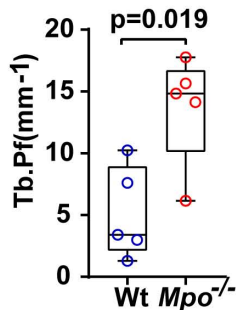
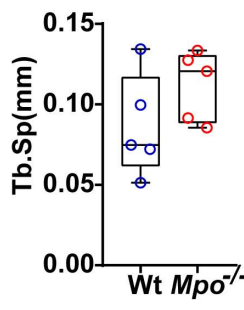
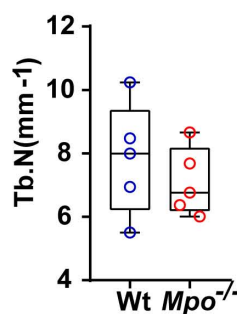
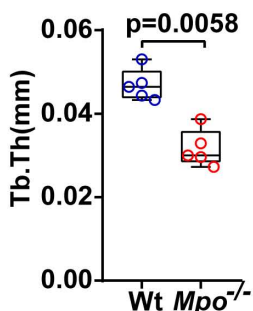
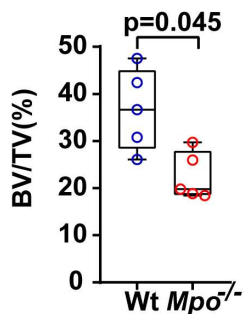
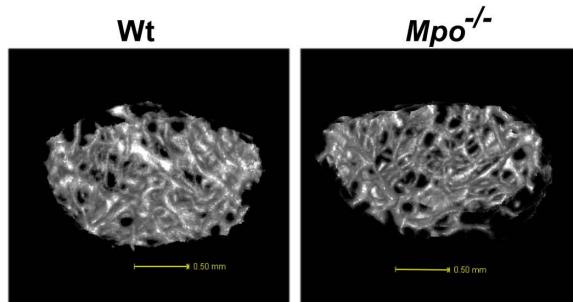


Figure 3

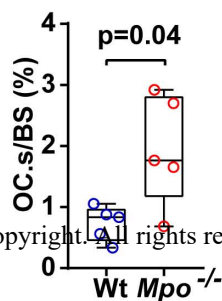
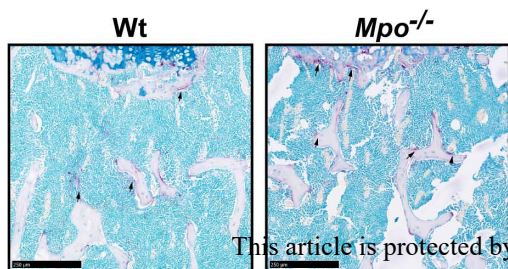
A



B



E



F

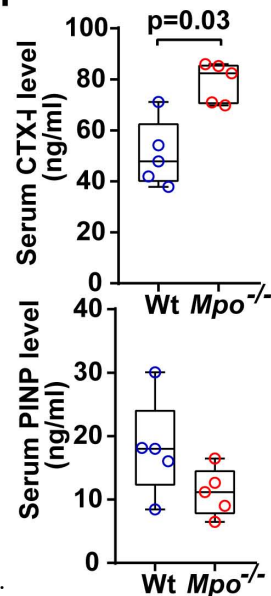


Figure 4

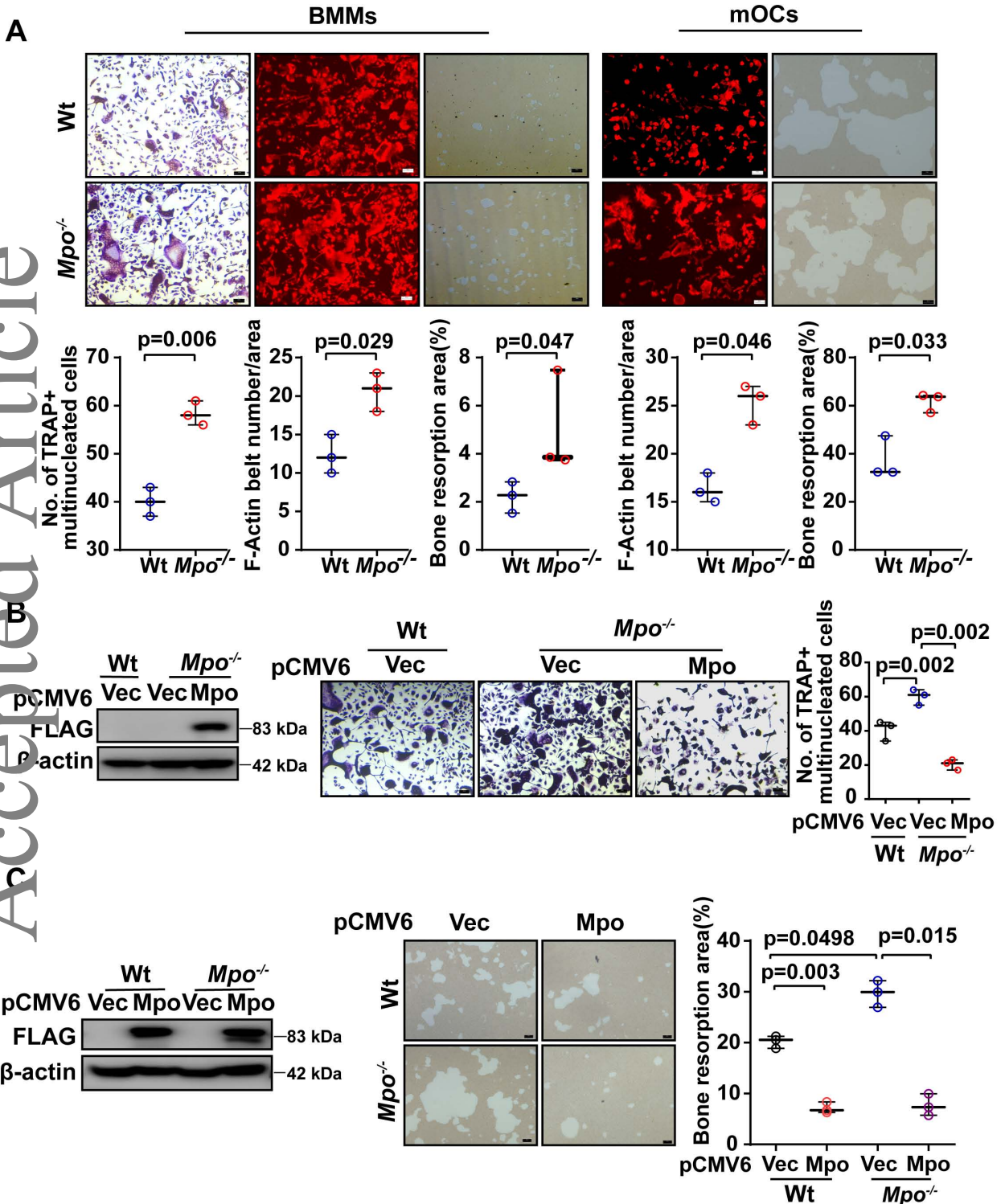


Figure 5

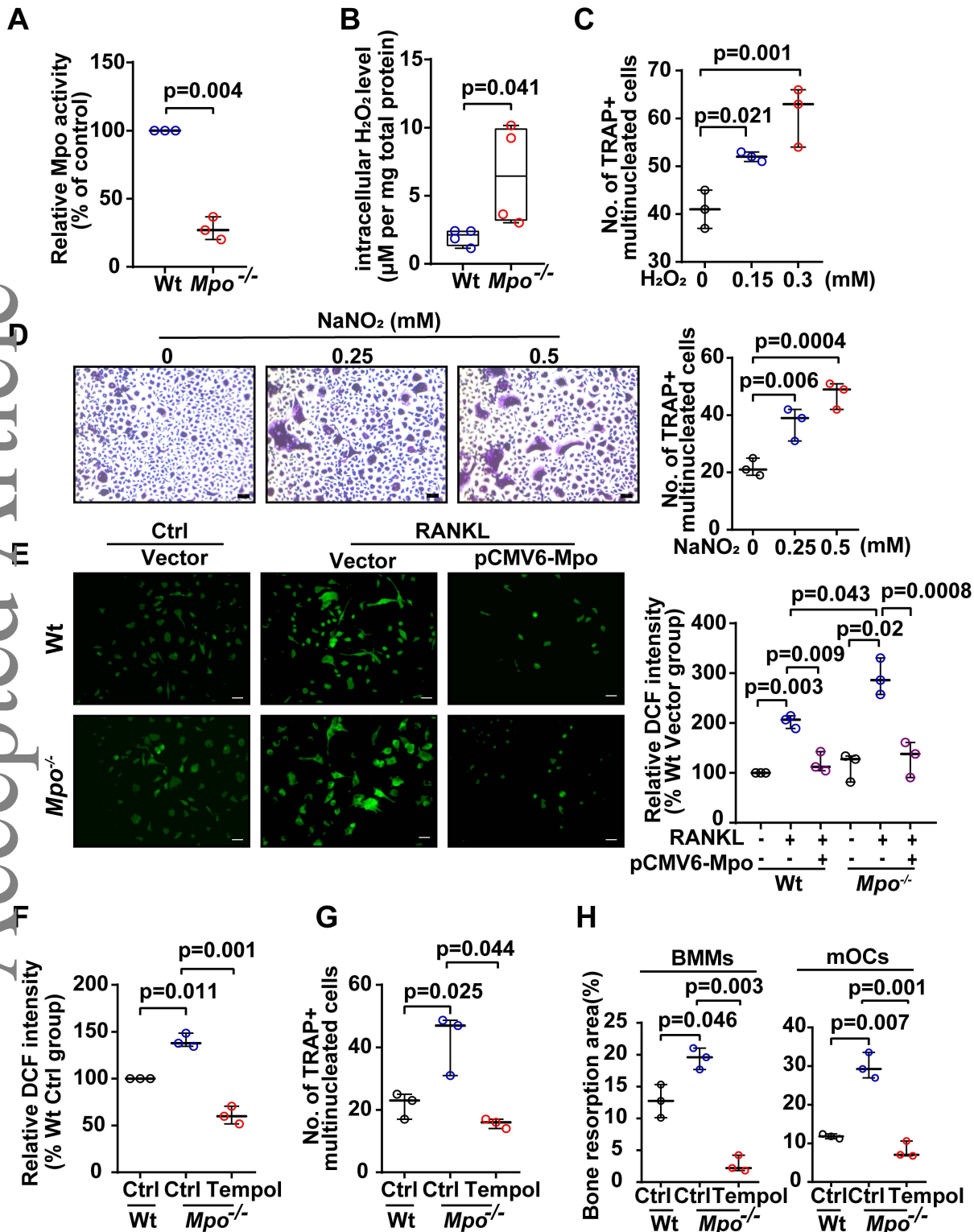


Figure 6

